Hyperpolarized water as an authentic magnetic resonance imaging contrast agent

Evan R. McCarney*†, Brandon D. Armstrong§, Mark D. Lingwood*, and Songi Han*†¶

Departments of *Chemistry and Biochemistry and §Physics and †Materials Research Laboratory, University of California, Santa Barbara, CA 93106

Communicated by Alexander Pines, University of California, Berkeley, CA, December 5, 2006 (received for review September 24, 2006)

Pure water in a highly ^{1}H spin-polarized state is proposed as a contrast-agent-free contrast agent to visualize its macroscopic evolution in aqueous media by MRI. Remotely enhanced liquids for image contrast (RELIC) utilizes a ^{1}H signal of water that is enhanced outside the sample in continuous-flow mode and immediately delivered to the sample to obtain maximum contrast between entering and bulk fluids. Hyperpolarization suggests an ideal contrast mechanism to highlight the ubiquitous and specific function of water in physiology, biology, and materials because the physiological, chemical, and macroscopic function of water is not altered by the degree of magnetization. We present an approach that is capable of instantaneously enhancing the ^{1}H MRI signal by up to 2 orders of magnitude through the Overhauser effect under ambient conditions at 0.35 tesla by using highly spin-polarized unpaired electrons that are covalently immobilized onto a porous, water-saturated gel matrix. The continuous polarization of radical-free flowing water allowed us to distinctively visualize vortices in model reactors and dispersion patterns through porous media. A ^{1}H signal enhancement of water by a factor of −10 and −100 provides for an observation time of >4 and 7 s, respectively, upon its injection into fluids with a T_1 relaxation time of >1.5 s. The implications for chemical engineering or biomedical applications of using hyperpolarized solvents or physiological fluids to visualize mass transport and perfusion with high and authentic MRI contrast originating from water itself, and not from foreign contrast agents, are immediate.

angiography | hyperpolarization | Overhauser effect | perfusion imaging

> Water is the driver of nature.
> Leonardo da Vinci

In a world where water is so ubiquitous and vital, the exchange and transport characteristics of water are fundamental for the function of an endless range of biological and industrial processes: blood physiology, protein folding, plant metabolism, biomaterial function, and oil recovery from reservoir rocks are only drops in the bucket. However, there exists a paucity of analytical tools capable of directly tracing and quantifying the transport and function of water through these already-water-saturated materials in a chemically selective and noninvasive manner. Although NMR and MRI are the best tools for this purpose, they face two main challenges. One is the lack of sensitivity inherent to all NMR experiments, especially for *in vivo* NMR studies of transport in biological and biomedical samples. A general approach to this sensitivity issue is the employment of high magnetic fields and cryoprobes, which is not only expensive technology but also is limited to <1 order of magnitude improvement in sensitivity. The other challenge is the lack of contrast, e.g., between the flowing water molecules being traced and the bulk water or water contained in the specimen. Current perfusion MRI techniques that address this contrast issue are dynamic susceptibility contrast-enhanced imaging (1, 2) and proton electron double-resonance imaging (PEDRI), also known as Overhauser MRI (3–9), both of which rely on paramagnetic molecules or ions to provide the water of interest with a different, detectable, physicochemical property and ultimately the desired contrast. However, such tracers are invasive, somewhat toxic, and do not precisely reflect the properties of water. Existing methodologies to achieve "authentic" contrast of fluid flow with no tracers are based on modulation of the polarization of inflowing water to distinguish it from the bulk water [NMR angiography (10), artery spin labeling (11), and NMR time-of-flight remote detection (12)], but the limitation is that the maximum modulation obtained is the inversion of polarization. Additionally, the NMR phase can be used to distinguish between still and moving molecules (11), but it is a rather time-consuming technique and thus not sensitive to time-variant flow dispersion evolving in time and space. We address both challenges by applying highly ^{1}H signal-enhanced water at 0.35 tesla (T) as a unique contrast agent to quantify and visualize the development of flow patterns and dispersion by NMR imaging. Because the ^{1}H signal of water is enhanced outside the sample and subsequently injected into the sample to maximize flow and perfusion contrast of the entering fluid, we named our approach "remotely enhanced liquids for image contrast" (RELIC). A 10- or 100-fold polarization enhancement in a 0.35-T field corresponds to the thermal polarization achieved in 3.5- or 35-T magnets, with 21 T being the highest commercially available NMR magnet, which shows the great potential of the proposed methodology. However, even in the case where signal enhancement at 0.35 T only amounts to a polarization that can be obtained by employing existing high magnetic fields, e.g., an enhancement factor of 10 corresponds to polarization that can be achieved at 3.5 T, the extremely high contrast between inflowing and bulk water of RELIC cannot be simply achieved with higher magnetic fields or other conventional approaches. This is because the employment of a high magnetic field alone only increases the absolute sensitivity but not the contrast between flowing and bulk fluid.

Contrast through the hyperpolarization, i.e., achieving higher than equilibrium polarization, of ^{1}H nuclear spins of water is a noninvasive method because the physical, chemical, and biological function of water remains unchanged, the same way that the function of thermally polarized water in a magnetic field of an MRI scanner is not altered from that in Earth's magnetic field. The nuclear ^{1}H spin hyperpolarization arises through the transfer of the orders of magnitude higher electron spin polarization within the same magnetic field; the electron and nuclear spin system is coupled through motion-mediated relaxation processes in solutions. This principle is known as dynamic nuclear polarization (DNP), or the Overhauser effect. The DNP mechanism generally states that in a system of two interacting spins (here protons and free electrons), the perturbation of the electron spin's polarization will change the population distribution be-

Author contributions: E.R.M., B.D.A., and S.H. designed research; E.R.M., B.D.A., M.D.L., and S.H. performed research; E.R.M., B.D.A., M.D.L., and S.H. contributed new reagents/analytic tools; E.R.M., B.D.A., M.D.L., and S.H. analyzed data; and E.R.M. and S.H. wrote the paper.

The authors declare no conflict of interest.

Abbreviations: ESR, election spin resonance; TEMPO, 2,2,6,6-tetramethylpiperidine 1-oxyl; DNP, dynamic nuclear polarization; ID, inner diameter; RELIC, remotely enhanced liquids for image contrast; PTFE, polytetrafluoroethylene.

¶To whom correspondence should be addressed. E-mail: songi@chem.ucsb.edu.

tween the proton spin energy levels (13–15). For DNP, or the Overhauser effect, in solution samples, perturbation is provided through the saturation of the electron spin resonance (ESR) transition, which will lead to nonequilibrium nuclear spin polarization that approaches the electron spin polarization driven by relaxation mechanisms involving simultaneous flips of the electron and the nuclear spin. In situations where the electron–nucleus system can be approximated as a two-spin system leading to four interacting energy levels, with that electron–nucleus interaction being the dominant relaxation pathway for the nuclei, the NMR signal enhancement, E, follows (15)

$$E = 1 - fs\rho\frac{|\gamma_S|}{\gamma_I}. \quad [1]$$

Here, ρ is the coupling factor that describes the interaction between the electron and proton, f is the leakage factor that describes the electron's ability to relax the proton, s is the saturation factor that describes the saturation of the electron Zeeman transition, and γ_S and γ_I are the magnetogyric ratios of the electron and proton, respectively.

Electron spins are usually provided by the unpaired electrons of dissolved or dispersed stable radicals. However, we have developed matrix-bound stable radicals that have highly efficient DNP performance in static and continuous-flow systems, because of their high concentration and mobility, without separating themselves from the matrix into the flowing water. Radical-free ^{1}H-hyperpolarized water therefore can be created as it flows through the matrix and is continuously or pulsewise fed into the system under investigation. This technique allows for the visualization of vortices in flow reactors, heterogeneous flow dispersion in porous media packing of separation columns, or perfusion patterns of blood circulation. To demonstrate the potential applicability of our development, we spatially tracked the flowing path of water in two different systems: one being a model reactor vessel with characteristic geometry containing pure water and the other being a packing of molecular sieves in water. Using 2D spin warp NMR imaging techniques (11), we visualize the macroscopic flow patterns such as vortices and convection for the former and mechanical dispersion for the latter, showcasing this methodology's capability to highlight water's flow within water and water-saturated materials.

Results and Discussion

We set up a DNP system using a magnetic field of 0.35 T, microwave frequency of 9.8 GHz, and proton frequency of 14.8 MHz and successfully amplified the ^{1}H NMR signal of water by a factor of −45 (data not shown) by using 2,2,6,6-tetramethylpiperidine 1-oxyl (TEMPO) derivatives as the free radical source, with the projected maximum enhancement (16) to be a factor of −137 (the maximum enhancement factor can be obtained by measurements of E at various microwave power irradiations contained in s of Eq. **1**). Using the deuterated ^{15}N-substituted TEMPO derivatives, we enhanced the ^{1}H signal of water by a factor of −73 and projected the maximum enhancement to be −157-fold. The discrepancy between actual and maximum signal enhancement is because our current technology does not permit complete saturation of the ESR transitions of TEMPO-based radicals, which is a surmountable problem when high-power microwave amplifiers (with ≈1-W output at 8–10 GHz) are used. The negative sign of the enhancement is due to the characteristics of dipolar relaxation governing the DNP enhancement (15).

We extended our static DNP setup to a continuous-flow system that combines DNP, water injection, and NMR imaging to demonstrate NMR flow-contrast imaging by using ^{1}H hyperpolarized water as a contrast agent (Fig. 1). The protons of water become hyperpolarized as they flow through radical-containing gel-filtration media situated inside a square TE_{102} X-band ESR

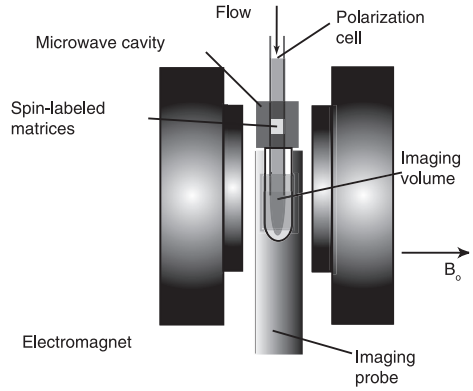

Fig. 1. Experimental setup for contrast MRI using continuously flowing hyperpolarized ^{1}H water. A syringe pump drives the water flow through the polarization cell situated inside the microwave cavity where microwave radiation saturates the ESR transitions of radicals immobilized on a gel matrix. The ^{1}H signal of water gets instantaneously hyperpolarized upon the transfer of polarization from the radicals and is then introduced into the sample cell contained inside an imaging probe equipped with gradients, where NMR image acquisition takes place. Water flows back out of the imaging area through the microwave cavity into a water reservoir.

cavity (Bruker, Billerica, MA) receiving 200 mW microwave power with a quality factor of 2,500. The water then flows into a water-saturated sample situated inside an NMR imaging probe with a central imaging plane separated from the center of the ESR cavity by 90 mm and flows back out.

TEMPO radicals are conjugated to the agarose-based gel filtration matrix (GE HealthCare, Piscataway, NJ) via stable peptide bonds, which leaves the eluant water perfectly radical-free when it flows out of the polarization cell. The matrix's characteristics allows for the instantaneous (<1 s) and effective ^{1}H polarization of water while continuously flowing at rates between 0.5 and 1.5 ml/min inside a 1-mm inner diameter (ID) column. The propogation of microwave radiation is perpendicular to the flow of the water, allowing the water to enter at the top and exit through the bottom of the cavity. Because the water is radical-free, it retains the hyperpolarization for the lifetime of the nuclear spin polarization of distilled water, after an exponential decay with a time constant of ≈2.7 s (spin-lattice relaxation time, T_1). By attenuating the microwave irradiation, the hyperpolarization can be turned off instantaneously, and the ^{1}H spin of water returns to its thermal equilibrium polarization at the magnetic field of 0.35 T. It is remarkable that the hyperpolarization and therefore the NMR contrast can be turned on and off or even fine tuned without physically altering the system by simply adjusting the microwave power. Therefore, we are able to noninvasively control the contrast of the ^{1}H NMR signal of water without changing its physicochemical property and without the addition of foreign contrast agents.

The capability to continuously create radical-free hyperpolarized water makes the limited observation time (given by T_1 of the hyperpolarized fluid) provided by RELIC less severe than it initially appears because high polarization of water with long T_1 times can be achieved. In pure water with a T_1 of 2.5 s, a −10-fold hyperpolarization already provides an observation time of 6 s, whereas an inverted signal, which is the maximum modulation achievable in conventional MRI methods, only allows for 1.7 s of observation time (Fig. 2). Given that the maximum expected enhancement is a factor of −157, it is reasonable to assume that approximately −100-fold ^{1}H signal-enhanced water can be introduced into the sample even when taking into account the T_1 relaxation as the fluid travels from a polarization cavity to the injection location. So, e.g., a saline solution with −100-fold

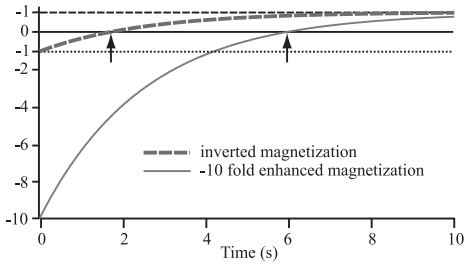

Fig. 2. Recovery of magnetization that has been inverted (dashed blue line) compared with −10-fold enhanced (solid red line) with time constant T_1 = 2.5 s. The two arrows indicate the different time points where magnetization crosses zero at 1.7 and 6 s for the different magnetization recovery curves. In pure water with a T_1 of 2.5 s, a −10-fold hyperpolarization provides an observation time of 6 s, whereas an inverted signal, which is the maximum modulation achievable in conventional MRI methods, only allows for 1.7 s of observation time.

hyperpolarization injected into a medium with a T_1 of ≈1.5 s (typical value for physiological fluids) will also provide distinct contrast during an observation time up to ≈6–8 s before decaying through zero (characteristic image patterns originating from zero polarization transitioned from negative polarization will be discussed below).

We chose a simple reactor vessel to test our contrast imaging methodology. A phantom that constrains the water to a cylindrical reservoir in the upper part and two parallel channels in the lower part was created from a polytetrafluoroethylene (PTFE) plug to fit inside a cylindrical glass tube (ID = 4 mm), as can be seen below in the front and side view diagram (Fig. 3*A*), photograph (Fig. 3*B*), and 2D NMR spin-warp image (Fig. 3*C*) obtained in the *xz* plane without water flow. The stronger signal intensity of the upper water reservoir reflects the larger water volume projected along the *y* direction, and the rounded shape of the upper part of the image is due to severe field inhomogeneity in this region of the electromagnet. The flow inlet and outlet capillaries (ID = 700 μm) are also depicted in the photograph, where the shorter capillary in the upper reservoir is the inlet and the longer capillary reaching into one of the channels is the outlet for the imaging experiments presented in Fig. 4*A*. Flowing water (between 0.5 and 1.5 ml/min) shows slightly higher NMR image intensity (Fig. 4*A*; MW = off) than static water (Fig. 3*C*) as it carries polarization that is less depleted by radio frequency pulses, which is due to the repetition delay being shorter than the ^{1}H spin relaxation time back to equilibrium (less than the ideal waiting time of $5 \cdot T_1$ = 13.5 s was used because of finite sample volume restrictions). This circumstance leads to a T_1 weighted contrast in Fig. 4*A* (MW = off)

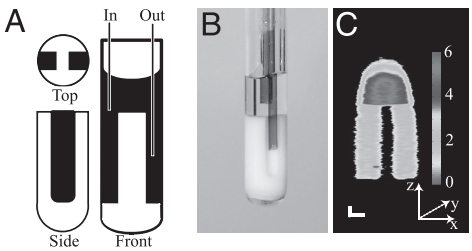

Fig. 3. Sketch (*A*), photograph (*B*), and static MRI (*C*) of the sample vessel used for contrast flow imaging presented in Fig. 4*A*. (*A*) The sketch depicts the PTFE phantom in white and the water in black. (*B*) The photograph shows the side view with the inlet capillary above the phantom and the exit capillary inside the channel. (*C*) The image is an *xz* projection with the long dimension *z* frequency encoded and the short dimension *x* phase encoded. [Scale bar: 1 mm (with different scales in the *x* and *z* directions).]

where the pathway of the water entering the upper reservoir, reaching into the channel on the right-hand side and back out, is indirectly visualized.

While water is flowing, the cavity is tuned to the center line ESR frequency of the nitroxide radical providing the maximum power output of our microwave source (200 mW), leading to partial ESR saturation of the radical and subsequent amplification of the ^{1}H signal of the flowing water. Note that the polarization of the water as it exits the microwave cavity is inverted, as mentioned above, and that greater amplification is observed with increasing flow rates. When the spins reach the sample quicker, the polarization has less time to decay on the relaxation time scale of radical-free water ($T_1 \approx 2.5$ s) before it enters the sample reactor (increasing flow rates from 0.5 to 1.5 ml/min in Fig. 4*A*). As time progresses, the NMR signal of the water continues to decay exponentially toward the equilibrium value. We can therefore track the flow of water by observing the gradually decaying negative signal as it leaves the inlet capillary (left-hand side of Fig. 4*A*), travels across the upper reservoir, enters the narrow channel and finally is forced out toward the exit capillary (right-hand side of Fig. 4*A*). The increasing black region at the location where the outlet arm of the capillary is placed originates from zero signal amplitude, resulting from the decay of the originally negatively polarized signal. Slower flow rates provided a more accurate picture of the flow dispersion near the inlet capillary, because at higher flow rates the distance traveled during the echo and acquisition time of the image pulse sequence falsifies the intensity distribution. This explains the 1- to 2-mm downstream shift of the most intense signal at higher flow rates (Fig. 4*A* at 1.0 and 1.5 ml/min).

The fast flow entering the vessel and bouncing off the PTFE phantom leads to vortex-like macroscopic flow patterns, which gradually become more distinct at higher flow rates (Fig. 4*A*; 1.5 ml/min). We have observed larger vortices in a vessel where the water does not flow through any channels (Fig. 4*B*). The water's flow path entering through the capillary, bouncing off the bottom of the vessel, splitting in two directions, and then turning around and flowing out of the vessel was unambiguously visualized. Such flow patterns are extremely difficult to experimentally observe without the use of exogenous contrast agents (e.g., dye molecules), which may change the flow property; they are only applicable for slow and stable flow patterns and are not applicable for biological samples.

To visualize the image region flooded by hyperpolarized liquids, of which the signature initially has negative amplitude, we created a phase map that only displays positive vs. negative signal amplitude. The voxels originating from inverted polarization contain 180° phase-shifted NMR signal when detected as transverse magnetization. In other words, a $\pi/2$ pulse with a given phase information will turn thermally polarized nuclei, which possess positive polarization (aligned with the *z* axis), into transverse magnetization along the *y* axis and DNP nuclei, which possess negative polarization (aligned with the $-z$ axis), along the $-y$ axis. This phase shift of π is displayed in a phase map, which shows the spatial occupation of the negatively polarized water as it enters the cell (the image at the far right of Fig. 4 *A–C* is obtained by calculating the phase difference between the images with the microwave on and off). Such a phase map can be used to interpret flow contrast with less ambiguity, e.g., whether intensity near zero originates from low fluid density or from flowing water with negative polarization that has decayed to nearly zero.

Another model system that we studied is the flow of water into a packing of 8–10 mesh molecular sieves, where more geometrical hindrance and therefore greater mechanical flow dispersion exists (Fig. 4*C*). In this sample, the inlet capillary reaches deeper into the sample (far right side Fig. 4*C*) and the outlet capillary (left side of Fig. 4*C*) is placed so that water is forced to find its

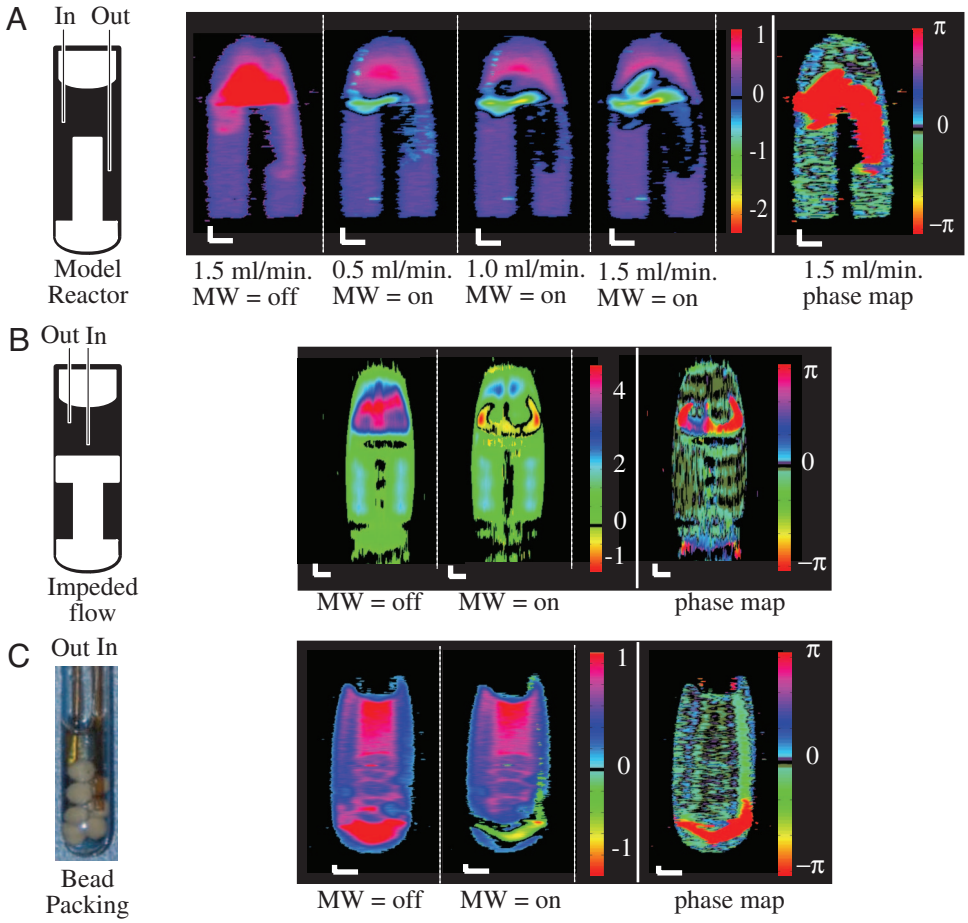

Fig. 4. Contrast flow imaging using ^{1}H hyperpolarized water. (*A*) Contrast flow imaging using ^{1}H hyperpolarized water in the sample vessel depicted in Fig. 3 at varying flow rates between 0.5 and 1.5 ml/min. (Scale bar: 1 mm along both axes.) The first image is without microwave irradiation under a continuous water flow of 1.5 ml/min (MW = off). The next three are contrast images using strong microwave irradiation, where flow rates of 0.5, 1, and 1.5 ml/min were used (MW = on). A phase map (shown in the final image of the series) distinctively shows the flow path of negatively hyperpolarized water. The characteristics and structure of the flow path of water, which enters at the left side of the vessel, then travels across the tube and down into the right channel, and finally exits into the outlet capillary, is visualized. (*B*) Contrast flow imaging using ^{1}H hyperpolarized water in a sample vessel without channels connected to the main reservoir, as depicted in the sketch (*Left*), with the water entering through the longer, center capillary tube. (*Right*) An image is shown without microwave (MW = off) irradiation under continuous water flow, and a contrast image using strong microwave irradiation (MW = on) with a flow rate of 1.5 ml/min. A phase map distinctively shows the flow path of negatively hyperpolarized water. The creation of vortex structures due to characteristic vessel geometry can be seen. (*C*) Contrast flow imaging using ^{1}H hyperpolarized water over a packing of submerged molecular sieve beads (shown in the photograph; *Left*). (*Right*) First is an image without microwave irradiation under continuous water flow (MW = off), and next is a contrast image using strong microwave irradiation, where a flow rate of 1.5 ml/min was used (MW = on). A phase map distinctively shows negatively hyperpolarized water. The water can be seen entering at the right side of the vessel, and then it travels below the bead packing, across the tube, and then back up into the outlet capillary.

way around the molecular sieve beads and flow upward to the outlet. This model experiment intends to demonstrate the utility of our contrast imaging technique for flow through restricted and complex media including separation columns, reactors packed with solid catalyst, or biological tissues. The first image, acquired while flowing and without microwave, depicts density contrast where the ^{1}H image intensity is reduced because of the presence of molecular sieves (Fig. 4*C*, MW = off). Also, one notices an air bubble trapped just to the left of the inlet tip where the signal intensity is also reduced. When the microwave, and therefore the contrast, is turned on, we again see inverted signal at the inlet capillary (Fig. 4*C*, MW = on). The decay of the signal clearly shows the path of the water out of the inlet capillary along the bottom of the tube around the beads toward the outlet capillary. The phase map further confirms the pathway of the inflowing hyperpolarized water through phase values of $\pm\pi$ that reveal the presence of the negatively polarized water (Fig. 4*C*, phase map). The further recovery through zero back to positively polarized equilibrium cannot be seen in the phase map because the phase between returning and equilibrium polarization is the same. This pattern is confirmed by comparing the coinciding zero intensity around the contrasted region of the contrast imaging of Fig. 4*C* (MW = on).

As can be seen in the obtained image contrast (see scale of color bars in Fig. 4), our current continuous-flow DNP setup only allowed for the use of −3- to −5-fold ^{1}H signal-enhanced water as a contrast agent at the time of injection. Therefore, the presented contrast images prove the principle of, but do not take advantage of the full potential of, our methodology. However, the discrepancy between the optimal and the presented setup is of surmountable technological nature. The introduction of higher microwave power at 9.8 GHz for full saturation of the ESR transitions of TEMPO as well as the use of more expensive deuterated or ^{15}N-substituted TEMPO derivatives will lead to higher Overhauser enhancement. More importantly, we are presently only using a small fraction of this low microwave output power. Because the ESR cavity had to be raised by ≈60 mm from its original location to accommodate the NMR probe at the

homogeneous location of the electromagnet, the ESR lines of the TEMPO radicals become greatly broadened by field inhomogeneous, diminishing the ESR saturation factor significantly. Additionally, because of the design of the exterior of the commercial ESR cavity and imaging probe, the distance between the center of the polarization and NMR detection could not be made shorter than 90 mm, leading to signal decay as the water travels between the two. Lastly, as mentioned in *Materials and Methods*, our imaging setup only allows us to obtain 2D images that are averaged over the entire depth dimension, thus greatly reducing the apparent signal enhancement factor and contrast.

We present a unique methodology to selectively and significantly enhance the ^{1}H NMR signal of the injected water so that it manifests a distinctly contrasted NMR signal from the bulk water. We successfully visualize flow patterns on model systems, supporting the use of this tool for flow tracking in model reactors and separation columns. RELIC offers the capability to track molecules by using highly enhanced NMR signal with ≈1 s time resolution with the option of turning this authentic contrast on and off repeatedly. These characteristics present a unique and powerful prospect for NMR imaging of flow dispersion and perfusion through materials and reactors. This is an important development because the study of spatiotemporal flow dispersion is fundamental for the understanding of a wide variety of chemical engineering processes, such as mass transport, filtration, separation, extraction, heterogeneous reactions, oil recovery, and contaminant percolation characteristics.

Furthermore, this unique MRI contrast mechanism is readily adaptable to biomedical applications such as blood and tissue perfusion MRI *in vivo*. Using our methodology, the *ex vivo* production of hyperpolarized infusion fluids and continuous *in vivo* injection, e.g., into small animal subjects, will allow for MRI scanning during a 7- to 11.5-s (for T_1 = 1.5–2.5 s) observation time. Hyperpolarization can take place within the same magnetic field and can be performed at a much less homogeneous region of the magnet compared with MRI. A magnetic field of 0.3–1.5 T is a reasonable choice for the proposed methodology because both the DNP efficiency as well as the MRI quality is high. At the lower field of 0.3 T, the DNP efficiency is higher, but usually the MRI resolution is lower. However, for MRI of susceptibility broadened heterogeneous tissues, the lower field offers less severe image distortions. At 1.5 T, we predict the DNP efficiency to be reduced by a factor of ≈4–5 [assuming pure translational motion and dipolar coupling (15)], but a higher signal-to-noise ratio and resolution for imaging of soft tissues is expected. Because MRI normally utilizes the abundant ^{1}H signal of water, the main limitation is not the low signal-to-noise ratio, but the low contrast-to-noise ratio that prohibits accurate blood flow tracking or visualization of poorly perfused tissue regions resulting from tumors. The introduction of highly polarized, yet radical-free, physiological fluids into the cardiovascular system or tissues *in vivo* promises great potential for fluid molecule tracking and perfusion MRI with high and authentic contrast from the fluid itself.

Materials and Methods

Immobilization of Radicals. NHS-Sepharose 4 Fast Flow (GE HealthCare) was washed with 10–15 volumes of 1 mM HCl at 4°C then reacted with 250 mM 4-amino-TEMPO (Sigma–Aldrich, St. Louis, MO) in 0.2 M $NaHCO_3$/0.5 M NaCl (pH 8.3) buffer at 4°C overnight. The total reaction volume was ≈150% of the matrix volume. The excess radical was washed with deionized water and stored at 4°C in 30% ethanol. Before use, the matrix was washed thoroughly.

Flow Setup. Spin-labeled Sepharose was loaded into the quartz polarization cell [2 mm outer diameter (OD); 1 mm ID] and centered in the microwave cavity (Fig. 1). A syringe pump was used to flow water through the microwave cavity where it was transiently polarized via the Overhauser effect. The polarized water then entered the imaging cell through a septum and flowed through capillary tubing (0.8 mm OD; 0.6 mm ID) into the water reservoir. The water exited the imaging cell through another capillary back through the microwave cavity. A PTFE phantom was machined to give a definite shape to the water signal (Fig. 3).

Overhauser Enhancement. The protons of water became hyperpolarized as they flowed through radical-bound gel filtration media when the center ESR line of the conjugated TEMPO radical was irradiated at 9.8 GHz. The matrix was centered inside a square TE_{102} X-band ESR cavity (Bruker) capable of 200-mW microwave power with a quality factor of 2,500 (Fig. 1). The cavity was inverted and raised 58 mm to allow the NMR coil to be positioned in the center (most homogeneous area) of the 0.35-T static field B_0. The concentration of spins in the Sepharose was estimated to be ≈10 mM by comparing the leakage factor (related to the relaxation rate of the water within the matrix) of spin-labeled Sepharose with known concentrations of free radical in solution. The enhancement of 10 mM radical free in solution was measured as a function of microwave power and used to estimate the maximum enhancement, approximately −170 fold (data not shown) (16). After hyperpolarization, the water flowed into to a commercial NMR imaging probe with a central imaging plane separated from the center of the ESR cavity by 90 mm. The water, after flowing through the polarization matrix, was tested for free radical presence by ESR, and the concentration of radical was shown to be well below detection limits.

NMR Imaging. A commercial NMR probe (Bruker) containing *x*, *y*, and *z*-gradients that is designed for use in a main static magnetic field (B_0) oriented along the long axis of the probe (*z* axis) was used for the imaging experiments in the ESR electromagnet, where the B_0 field is oriented perpendicular to the probe's long axis. Therefore, instead of using the dB_z/dz component of the *z* gradient (here, *z* is along the gravitational axis), its concomitant components were used for our experiment. The only relevant contribution to the imaging experiment in a main $B_{0,x}$ field is the dB_x/dx component contained in the *z* gradient (17). The dB_x/dx gradient was found to be linear within the length along the *x* axis relevant for our sample (data not shown) and have a gradient strength similar to that of the z gradient's amplitude, i.e., of dB_z/dz (18). Similarly, the *x* gradient provided dB_x/dz components for imaging in a $B_{0,x}$ field, again linear and 50% amplitude of the original *x* gradient. The *y* gradient cannot be used for imaging in an $B_{0,x}$ field because it contains all three concomitant gradient components along the $B_{0,x}$ axis. Therefore, in our current experimental setup, only imaging along the *x* and *z* axes can be performed with the possibility of simple and straightforward image reconstruction; however, this is due specifically to our system and is not a principle limitation.

A 2D spin warp imaging sequence based on spin echo detection was used. A total of 256 points along the direct, frequency-encoded direction and 32 points along the indirect, phase-encoded direction were used. The echo time (from the 90 pulse to the center of the echo) was 4.25 ms. A spectral width of 40 KHz and a frequency-encoded gradient strength of 0.102 T/m were used. The gradient pulse duration for the phase encoded gradient was 2 ms, and the gradient amplitude was 0.031 T/m. The $\pi/2$ pulse duration was 4.4 μs. The repetition time (time between end acquisition and beginning of next $\pi/2$ pulse) was 1 s, and 16 signal accumulation steps were used.

We thank Sandra Garcia and Erin E. McDonnell for their contribution, as well as Melanie Rosay for friendly support, during the initial efforts

in setting up the first DNP instrumentation at 0.35 T in our laboratory. This work was supported by the Dreyfus New Faculty Award and through the Materials Research Laboratory program of the National Science Foundation under Grant DMR00-80034.

1. Law M, Hamburger M, Johnson G, Inglese M, Londono A, Golfinos J, Zagzag D, Knopp EA (2004) *Technol Cancer Res Treatment* 3:557–565.
2. Wintermark M, Sesay M, Barbier E, Borbely K, Dillon WP, Eastwood JD, Glenn TC, Grandin CB, Pedraza S, Soustiel J-F, *et al.* (2005) *Stroke* 36:e83–e99.
3. Lurie DJ, Bussell DM, Bell LH, Mallard JR (1988) *J Magn Reson* 76:366–370.
4. Grucker D (1990) *Magn Reson Med* 14:140–147.
5. Golman K, Petersson JS, Ardenkjær-Larsen J-H, Leunbach I, Wistrand L-G, Ehnholm G, Liu K (2000) *J Magn Reson Imaging* 12:929–938.
6. Lurie DJ (2003) *Biol Magn Reson* 18:547–578.
7. Subramanian S, Matsumoto, K-i, Mitchell JB, Krishna MC (2004) *NMR Biomed* 17:263–294.
8. Lurie DJ, Davies GR, Foster MA, Hutchison JMS (2005) *Magn Reson Imaging* 23:175–181.
9. Li H, He G, Deng Y, Kuppusamy P, Zweier JL (2006) *Magn Reson Med* 55:669–675.
10. Nishimura DG, Macovski A, Pauly JM, Conolly SM (1987) *Magn Reson Med* 4:193–202.
11. Callaghan P (1991) *Principles of Nuclear Magnetic Resonance Microscopy* (Oxford Univ Press, Oxford).
12. Granwehr J, Harel E, Han S, Garcia S, Pines A, Sen PN, Song YQ (2005) *Phys Rev Lett* 95:075503/1–075503/4.
13. Overhauser AW (1953) *Phys Rev* 92:411–415.
14. Carver TR, Slichter CP (1953) *Phys Rev* 92:212.
15. Hausser KH, Stehlik D (1968) *Adv Magn Reson* 3:79–139.
16. Nicholson I, Lurie DJ, Robb FJL (1994) *J Magn Reson B* 104:250–255.
17. Blümich B (2000) *NMR Imaging of Materials* (Oxford Univ Press, Oxford).
18. Volegov PL, Mosher JC, Espy MA, Kraus RH, Jr (2005) *J Magn Reson* 175:103–113.